HEFAT2014
10th International Conference on Heat Transfer, Fluid Mechanics and Thermodynamics
14 – 26 July 2014
Orlando, Florida

TWO-PHASE FLOW BEHAVIOUR IN A SMOOTH HAIRPIN TUBE: ANALYSIS OF THE DISTURBANCE USING CAPACITIVE MEASUREMENTS

De Kerpel K.[a,*], De Keulenaer T.[b], De Schampheleire S.[a] and De Paepe M.[a]
*Author for correspondence

[a]Department of Flow, Heat and Combustion Mechanics
Ghent University-UGent, Sint-Pietersnieuwstraat 41
B-9000, Ghent,Belgium,
[b]INTEC/IMEC
Ghent University-UGent, Sint-Pietersnieuwstraat 41
B-9000, Ghent, Belgium
E-mail: Kathleen.DeKerpel@UGent.be

ABSTRACT

Two-phase refrigerant flow up-and downstream of a sharp return bend is studied. The capacitance of the flow is logged at several locations up-and downstream of the return bend. Analysis of the capacitance time traces is performed to evaluate the presence of a flow disturbance due to the bend. A vertically oriented bend is studied with an inner diameter of 8 mm and a radius of 11 mm. Smooth straight tubes with an internal diameter of 8 mm are connected to the in- and outlet of the return bend. Upward as well as downward directed flows are studied. The refrigerant R134a is used and the mass flux G and vapour quality x are varied between 200 and 400 kg/m²s and 0-1, respectively. A downstream disturbance up to 21.5D is observed for both up-and downward flow.

INTRODUCTION

In single phase flow, the effect of a return bend on the flow behaviour has been studied since the beginning of the 20th century. Eustice [1, 2] first studied the flow through a curved channel experimentally. Dean [3-5] was the first to make an analytical analysis of the flow through a curved channel and prove the existence of the secondary flows occurring in single phase flow through a curved channel.

The knowledge on the effect of a curved channel on two-phase flow behaviour is still quite limited. However this effect can be of importance for e.g. fin-and-tube heat exchangers, in these compact heat exchangers the tubes contain a considerable amount of sharp return bends. In the search for better heat exchangers designs, this topic has recently gained some attention. A number of studies are available on the two-phase flow behaviour in a return bend and its adjacent tubes for air-water flow [6-8] and for refrigerant two-phase flow [9-11]. However, all these studies asses the flow behaviour in the bend and up-and downstream of the return bend based on flow visualizations. This method renders a very good insight into the flow behaviour, since one can see what is happening. However, the analysis of these images is quite subjective and can only be used as a qualitative assessment. Further processing of the flow visualizations can allow for some quantitative assessment, as shown by De Kerpel et al. [9]. However, the precision of this method is limited and due to the large amount of data, quite computationally expensive.

NOMENCLATURE

C	[F]	capacitance
D	[m]	tube diameter
f	[Hz]	frequency
Fs	[Hz]	sample frequency
G	[kg/m²s]	mass flux
PSD	[-]	Power spectral density
R	[m]	U-bend radius
x	[-]	vapour quality
τ	[samples]	Scale

Subscripts	
L	Liquid
meas	Measured
norm	Normalized
V	Vapour

In this work, the flow up-and downstream of a return bend is studied based on the capacitance of the flow. This is a robust and low-cost option compared to flow visualizations.

Processing the time trace of the capacitance is also low in computational cost compared to image processing.

EXPERIMENTAL SETUP

The measurements are done on a test setup designed to generate two-phase flows at a given vapour quality x and mass flux G. More data on the setup itself can be found in [9, 12]. The experimental setup comprises a refrigerant loop, a hot water loop and a cold water loop. In this test setup, the refrigerant is partially evaporated to a desired vapour quality at a given mass flux G. This partial evaporation takes place in a tube-in-tube heat exchanger (preheater). The refrigerant flows through the central tube of the preheater, hot water flows in the annulus. The vapour quality at the outlet of the preheater can be controlled by varying the mass flow rate and temperature of the hot water in the annulus and the length of the preheater. The length of the preheater can be varied between 1 m and 15 m by adjusting shut-off valves. Downstream of the test sections, the refrigerant is condensed and subcooled using water from the cold water loop. For a refrigerant mass flux below 250 kg/m^2 s, the uncertainty is smaller than 1.5% and at a mass flux higher than 250 kg/m^2 s the uncertainty is smaller than 0.75%. For the vapour quality x, the uncertainty varied between ±0.005 and ±0.02. Temperatures are measured using a thermocouple (type K) with an accuracy of ±0.05 K . This accuracy was reached by an *in situ* calibration using a water triple point cell, more information about the calibration technique can be found in [12]. The pressure transducer used to record the inlet pressure of the test section has an accuracy of ±1.6 kPa.

A test section in the form of a hairpin tube is added to this setup for this work. A hairpin tube is basically a combination of two long straight parallel tubes interconnected by a sharp return bend.

Test Section

A test section under the form of a hairpin tube with capacitance sensors at several locations up-and downstream of the return bend is used. In Figure 1 a schematic representation of the test section is shown with an indication of the location of the sensors. The internal tube diameter is 8 mm and the bend radius 11 mm. The numbering of the sensors will be used as depicted in this figure throughout this work.

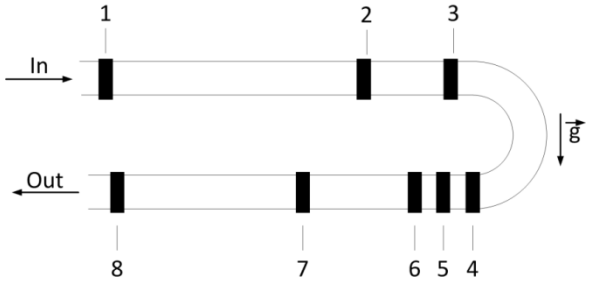

a) Downward flow

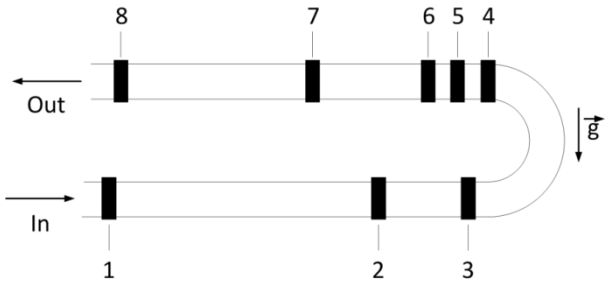

b) Upward flow

Figure 1 Sensor positions and numbers for down- and upward flow

The distance between the centre of the sensing electrode and the inlet/outlet of the bend is shown in Table 1. The distance is expressed in a number of tube diameters; the tube diameter is 8 mm.

Table 1 Distance between each sensor and the inlet/outlet of the bend expressed in a number of tube diameters. Upstream sensors have a negative distance.

Sensor	1	2	3	4	5	6	7	8
L [D]	-168.5	-18.5	-5.5	2.5	5.5	8.5	21.5	174.5

Capacitance Sensor

The capacitance sensor used to measure the capacitance time trace is based on the design by Canière et al. [12]. A cross section of the sensor construction is shown in Figure 2.

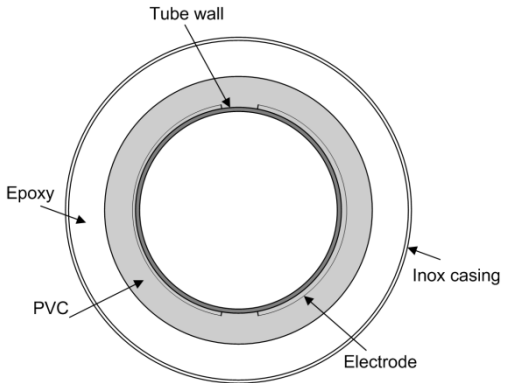

Figure 2 Sensor cross section

The capacitance is measured between two concave electrodes. The electrodes have an axial length of 8 mm and an angle of 160°. They are etched out of a flexible circuit material with a copper cladding (Ultralam 3850 (50µm) by Rogers Corporations®). The electrodes are glued to plastic parts for structural strength; this assembly is then placed in a metal casing and the gaps between the casing and the plastic parts are filled with an epoxy resin.

The capacitance between the two sensing electrodes is measured through an in-house made transducer. The transducer design is based on the circuit proposed by Yang et al. [13]. This transducer can measure a capacitance between 0 and 10 pF with

an accuracy of 4 fF. The output of the transducer is a voltage proportional to the capacitance (sensitivity 1.16 V/pF). The output voltage is logged with a DAQ system at a sample rate of 1 kHz.

CAPACITANCE TIME TRACES

The time traces are logged for each sensor at several mass fluxes and vapour qualities. Three main flow regimes are observed: slug flow, intermittent flow and annular flow. The measurements are conducted for upward flow as well as for downward flow. To allow an easy comparison between the capacitance time traces, the normalized capacitance is shown. This is calculated as:

$$C_{norm} = \frac{C_{meas} - C_V}{C_L - C_V} \quad (1)$$

In Eq.(1) C_{meas} stands for the measured capacitance, C_V is the capacitance for full vapour flow and C_L is the capacitance for full liquid flow.

In Figure 3 the time traces for sensor 1 and sensor 4 are compared for a G = 400 kg/m²s and x = 10%. The flow regime is slug. This is also evident from the capacitance time traces. For sensor 1 and sensor 4, the signal alternates between quite low capacitances and high capacitances. This is characteristic of the slug flow regime: large vapour bubbles are alternated with liquid slugs. Since the dielectric constant for the liquid phase is higher than that for the vapour phase, the capacitance for the liquid slugs is significantly higher than that for the vapour bubbles. The time traces for sensor 1 and sensor 4 are compared here because they are expected to show the largest differences. Sensor 1 is located far upstream of the return bend and can be thus assumed to be uninfluenced by the return bend. Sensor 4 is located close to the outlet of the bend and if a disturbance due to the bend is present, it will be the most intense at this location. Comparing the time traces for sensor 1 and sensor 4, it can be seen that for sensor 4 a more pronounced ripple is present in the low capacitance regions. This is most likely a consequence of the ripple on the vapour-liquid interface induced by the bend. This ripple was observed in flow visualizations by several authors [6, 8-10]. This ripple was also observed in the time traces for sensor 5 and sensor 6 for slug flows. These time traces are not shown here for simplicity.

In Figure 4 the time traces for sensor 1 and sensor 4 are again compared, however, for a higher vapour quality. For this figure, G = 400kg/m²s and x = 21%. The flow regime is intermittent flow. From this figure, no clear difference between the time traces can be observed. This is also the case for time traces recorded for annular flow, however, time traces for annular flow are not shown here for the sake of simplicity. Furthermore, no clear difference was seen between the time trace for sensor 1 and any other of the sensors for intermittent or annular flow.

However, that there is no visually observable effect present does not mean that there is no effect at all. Studies on the pressure drop in a hairpin tube downstream of the return end indicate that there is an elevated pressure drop up to at least 30D downstream of the bend for slug flow as well as for annular flow and intermittent flow [9, 14]. Since the two-phase pressure drop is a result of the two-phase flow behaviour [15], this elevated pressure drop is caused by an underlying disturbance of the flow. Hence, a disturbance due to the return bend is probably also present in intermittent flow and annular flow close to the outlet of the bend. The capacitance time traces are analyzed further in order to uncover a disturbance due to the bend in the following section.

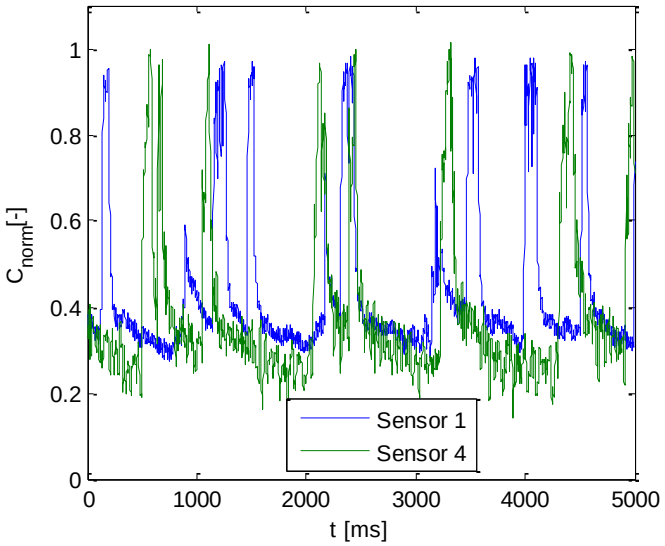

Figure 3 Capacitance time traces for downward slug flow, G = 400 kg/m²s and x = 10%. The time traces for sensors 1 and 4 are compared (sensor numbering according to Figure 1)

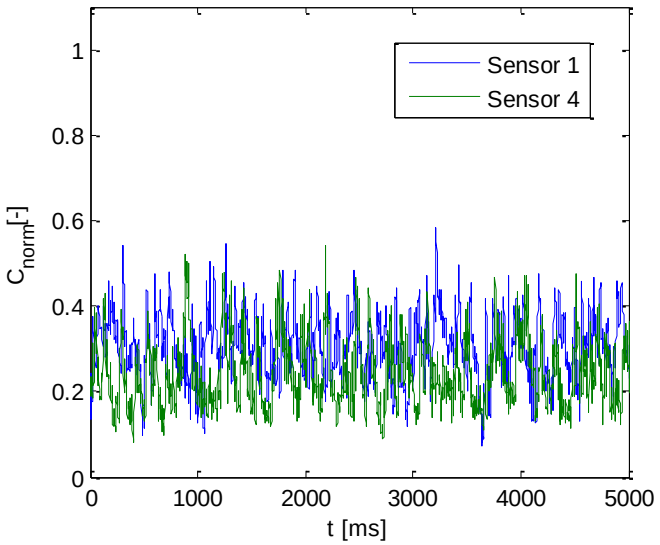

Figure 4 Capacitance time traces for downward intermittent flow at G = 400 kg/m²s, x = 21%

The results for upward flow are similar to the ones for downward flow. For slug flow the ripple for the low capacitance regions is more pronounced in the signals recorded close to the bend. For annular and intermittent flow no clear

difference between the time trace close to the bend and far up- or downstream of the bend can be observed visually.

DATA PROCESSING

As already stated in the previous section, a bend effect cannot be observed by comparing the capacitance signals visually for intermittent and annular flow. However, pressure drop measurements up-and downstream of a return bend suggest that a bend effect is indeed present. To uncover a possible bend effect the capacitance signals, wavelet analysis is used. For the sake of simplicity, the theoretical considerations on wavelet analysis are not discussed here, the interested reader is referred to the very instructive work of Percival and Walden [16] and to De Kerpel et al. [17] for an example of an application. The wavelet transform provides a multiscale analysis of a sequence of data points, for each considered scale τ, a set of wavelet coefficients is found as a function of time (in case of a time series). The wavelet coefficients itself are not studied here because it is not expected that the bend effect will have a time dependent effect on the signals. Based on the wavelet coefficients, an estimate of the power spectral density (PSD) of the signal can be calculated [16].

The frequency resolution in the PSD estimate depends on the sample frequency. The frequency linked to each scale τ can be calculated through Eq. (2).

$$f = \frac{1}{2\sqrt{2}\tau\Delta t} \tag{2}$$

In this equation, $\Delta t = 1/Fs$, where Fs is the sample frequency. The resulting frequencies for the considered case are shown in Table 2.

Table 2 Overview of the considered scales τ, the associated frequency f (calculated with Eq. (2)) and the matching octave band for each frequency.

τ [samples]	f [Hz]	$f_{band,low}$ [Hz]	$f_{band,high}$ [Hz]
1	353.55	250.00	500.00
2	176.78	125.00	250.00
4	88.39	62.50	125.00
8	44.19	31.25	62.50
16	22.10	15.63	31.25
32	11.05	7.81	15.63
64	5.52	3.91	7.81
128	2.76	1.95	3.91
256	1.38	0.98	1.95
512	0.69	0.49	0.98

In Figure 5 **PSD estimate based on the wavelet coefficients for G = 400kg/m²s and x = 21% , for downward flow**Figure 5 the PSD estimates for several sensor locations are compared for downward flow at G = 400 kg/m²s and x = 21%. The numbering of the sensors is according to Figure 1. In each of the subfigures of Figure 5, the PSD of a certain sensor location is compared to the PSD for sensor 1. This sensor is located far upstream of the bend where there is no bend effect, hence this sensor is used as a reference throughout this work.

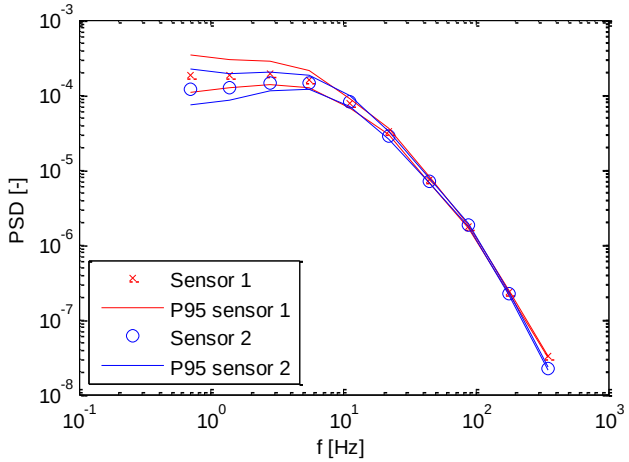

(a) PSD estimates for sensor 1 and sensor 2

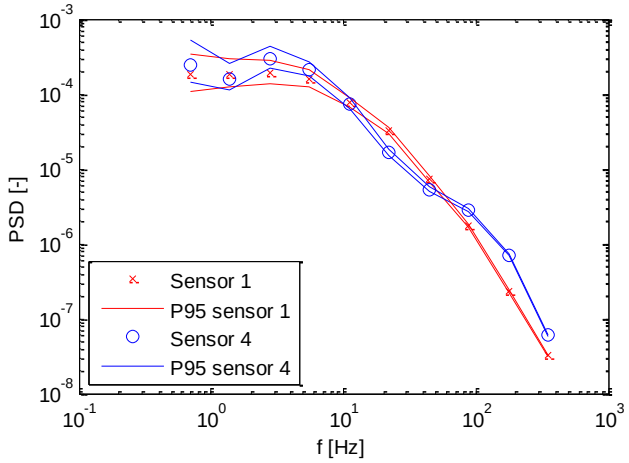

(b) PSD estimates for sensor 1 and sensor 4

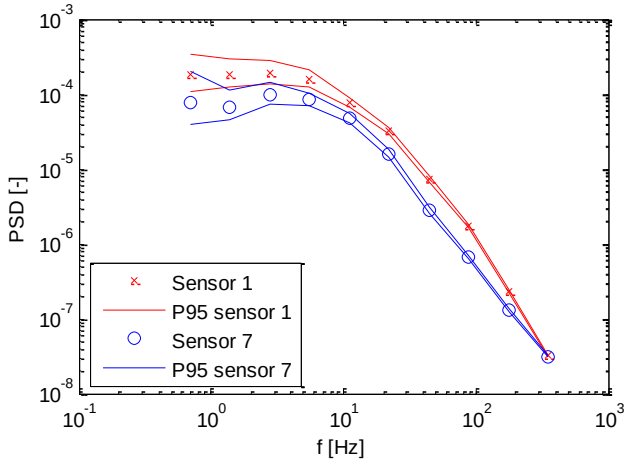

(c) PSD estimates for sensor 1 and sensor 7

Figure 5 PSD estimate based on the wavelet coefficients for G = 400kg/m²s and x = 21%, for downward flow. P95 indicates the 95% probability interval

Comparing sensor 1 with sensor 2 in Figure 5(a), one can see that there is no significant difference between the estimates,

except for the highest frequency (350 Hz), where there is a small significant difference between the estimates. Since most of the two-phase flow behaviour has a frequency content below 100 Hz [18], it is unlikely that this difference is induced by the bend. It is most likely due to high frequency noise picked up by the transducers [12]. In Figure 5(b), sensor 1 and sensor 4 are compared; these PSD estimates correspond to the signals shown in Figure 4. Sensor 4 is located close to the outlet of the bend and it is expected that the bend effect will be the most intense at this location. A significant difference between the two estimates is observed at several frequencies. In the medium frequency range, the PSD estimate of sensor 4 is significantly below the reference and for frequencies around 100 Hz it is significantly higher than the reference. Further downstream of the bend, at sensor 7, a significant effect between the PSD estimates can be seen.

Since the frequency content of the flow behaviour itself continuously changes depending on the mass flux G and the vapour quality x, the bend effect does not translate itself as a constant offset in the PSD estimate compared to the reference. This can be seen by e.g. comparing Figure 5 and Figure 6. If the vapour quality changes, the shape of the PSD estimate itself changes as well as the differences between the PSD estimates are shifted. In Figure 6 a similar comparison between the PSD estimates for several sensor locations is made for G = 400 kg/m² and x = 44%. In Figure 6(a), the PSD estimates for sensor 1 and sensor 2 are again compared. The shape of the PSD estimate is different compared to Figure 5(a). For the lowest frequencies (< 2 Hz), the values are similar. For the medium frequencies (between 2 Hz and 40 Hz), the slope of the PSD as a function of the frequency is very small. If the vapour quality increases, the vapour phase accelerates, gradually shifting the frequency content to higher frequencies. This explains the difference in shape between Figure 5 and Figure 6. Nevertheless, there is no significant difference between the PSD estimates for sensor 2 and sensor 1. Again, for the PSD estimates for sensor 1 and sensor 4, a significant difference can be observed. However, for this case, the PSD estimate is consistently below that for sensor 1. This is also the case for the PSD estimates for sensor 7 compared to the estimates for sensor 1.

Based on the specific cases in Figure 5 and Figure 6, it is expected that the bend effect for downward flow stretches up to at least the sensor location of sensor 7. For the upward flow a similar behaviour was observed. An example is shown in Figure 7. The results for upward flow are similar to the results for downward flow. Again, no significant effect is present between sensor 1 and 2. For sensors 4 and 7, a significant effect can be discerned, indicating that a bend effect is present to at least 21.5D downstream of the bend.

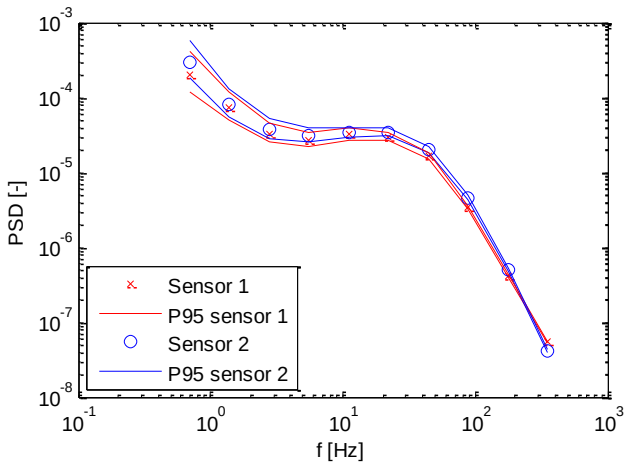

(a) PSD estimates for sensor 1 and sensor 2

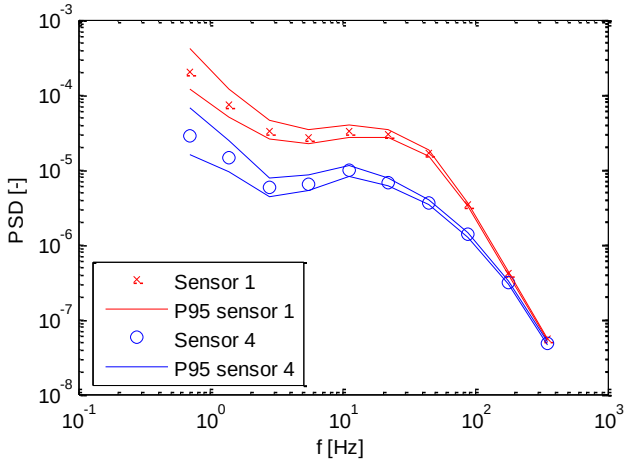

(b) PSD estimates for sensor 1 and sensor 4

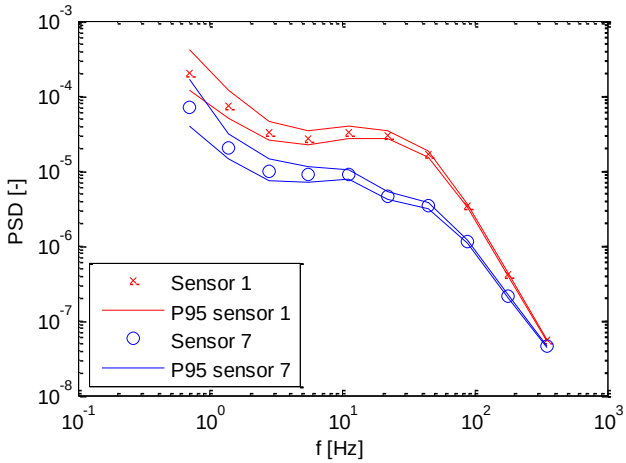

(c) PSD estimates for sensor 1 and sensor 7

Figure 6 PSD estimate based on the wavelet coefficients for G = 400 kg/m²s and x = 44%, for downward flow. Pair wise comparison between several sensor locations.

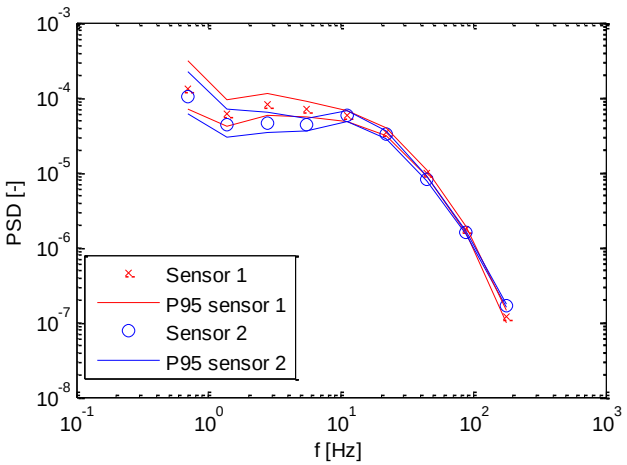

(a) PSD estimates for sensor 1 and sensor 2

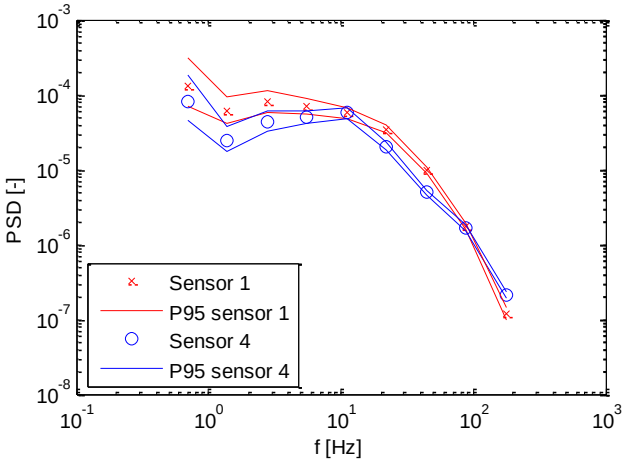

(b) PSD estimates for sensor 1 and sensor 4

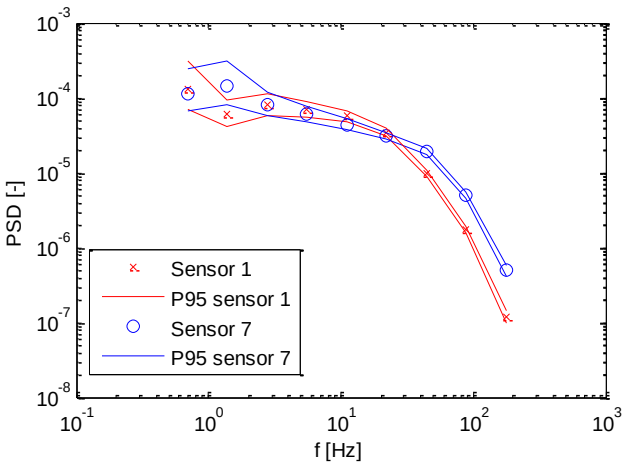

(c) PSD estimates for sensor 1 and sensor 7

Figure 7 PSD estimate based on the wavelet coefficients for G = 400 kg/m²s and x =35%, for upward flow. Pair wise comparison between several sensor locations.

However, not all measurements can be discussed here in detail as in Figure 5, Figure 6 and Figure 7. To get a view of the overall effect of the return bend on the flow behaviour, the PSD estimates associated with a specific frequency are plotted as a function of the vapour quality x. This is done in Figure 8 for downward flow for a frequency of 88 Hz and 22 Hz (Table 2). In Figure 8 (a) the values for sensor 1, sensor 3 and sensor 8 show a similar behaviour. Sensor 3 is located upstream of the bend and sensor 8 far downstream of the bend, hence it is expected that the return bend has little or no effect on the flow behaviour in these locations. This is confirmed in Figure 8 (a). Sensor 4 and sensor 7 are located at 2.5D and 21.5D downstream of the outlet of the bend, respectively. In Figure 8 (a) one can see that the PSD estimates for the considered frequency show a different behaviour as a function of x. This was also observed for sensor 5 and sensor 6, the data for these sensors is not shown here for simplicity. In Figure 8 (b) similar trends can be observed: sensor 1, sensor 3 and sensor 8 show a similar behaviour as a function of x. Sensor 4 and sensor 7 show a different behaviour as a function of x compared to the reference sensor (sensor 1). However, in Figure 8 (b) the difference between the 'affected' sensors (sensor 4 and sensor 7) and the 'unaffected' sensors is only evident for vapour qualities of 20% and above. In Figure 8 (a) the difference is evident for the full vapour quality range, especially for sensor 4. This is probably a consequence of the shift in the frequency content of the flow behaviour with varying x. For low vapour qualities, a large part of the frequency content is localised at low frequencies. A good example here is slug flow, where the frequency of the liquid slugs is dominant. As shown in Figure 3 the bend induces a ripple on the vapour-liquid interface and this adds to the higher frequency content of the signal. This is why, at the PSD estimates for 88 Hz, a significant effect is seen for the low vapour quality flows. However, the frequency content added by the disturbance of the bend at lower frequencies is not significant compared to the already dominant frequency content of the flow behaviour.

A final remark can be made about sensor 8. Although the PSD values follow the same trend as the values for sensor 1 and sensor 3, they are consistently lower than the values for sensor 1. At this point, it cannot be determined whether this is due to a bend effect. Nonetheless, due to the large distance between the bend outlet and sensor 8 and because the trends are consistently the same for sensor 1 and sensor 8 it can be assumed that the disturbance is limited, if it is present at all.

For the sake of simplicity, the PSD estimates as a function of x are not shown here for all considered frequencies (Table 2). For the frequency bands between 125 Hz and 7 Hz, a clear split could be observed between disturbed sensors close to the bend and undisturbed sensors. For higher and lower frequencies, no clear difference between the two groups could be discerned. This is in agreement with the finding by Schubring and Shedd [18] who found that the frequency content of two-phase flow is mostly located below 100 Hz.

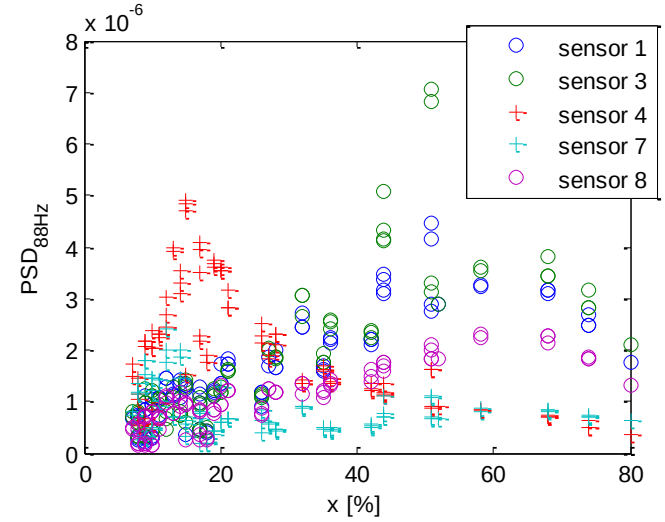

(a) PSD estimates for sensor for f = 88Hz, octave band 62,5Hz to 125Hz (Table 2)

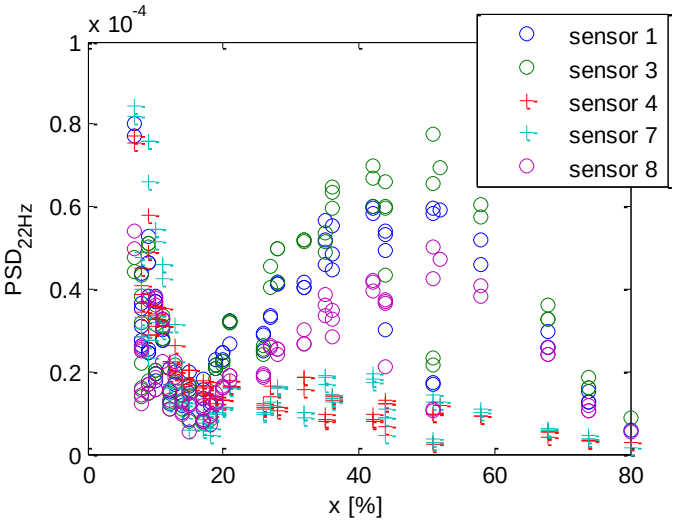

(b) PSD estimates for sensor for f = 22Hz, octave band 15 Hz to 3 1Hz (Table 2)

Figure 8 PSD estimate values for downward flow for a specified frequency as a function of the vapour quality x

For upward flow similar conclusions could be made. In Figure 9 the PSD estimate values for f = 44 Hz (octave band 31Hz – 62.5Hz) are shown as a function of the vapour quality. For sensor 4 the behaviour as a function of x is clearly different from the reference sensor 1. For sensor 7, the effect is less pronounced this could be a consequence of the fact that gravity acts in the opposite direction of the flow in the bend and hence reduces the intensity of the disturbance downward of the bend, causing it to damp out faster.

Another difference with the downstream case is the consistently lower values for sensor 3 compared to the reference sensor. Due to the gravity being aligned opposite to the flow direction, this could be an effect of the bend. Several authors have reported an effect upstream of the bend for upward flow [7, 10]. The effect is only observed for the higher frequency ranges (octave bands between 125 Hz to 31 Hz).

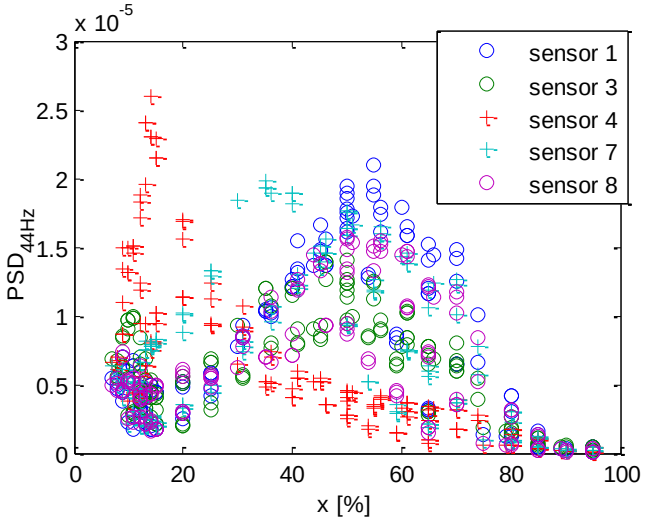

Figure 9 PSD estimate values for upward flow for f = 44Hz (octave band 31Hz – 62.5Hz) as a function of the vapour quality x

CONCLUSION

Capacitance time traces of two phase flow were analysed to uncover the effect of a sharp return bend on the flow behaviour up-and downstream of the return bend. A bend effect was observed up to 21.5D downstream of the bend for upward flow as well as downward flow. For upward flow, an indication of a limited disturbance 5.5D upstream of the bend was found. For downward flow, the disturbance possibly stretches out up to 174D downstream of the bend. Further research is necessary to assess whether the disturbance actually stretches this far downstream of the bend.

REFERENCES

[1] Eustice J., Flow of water in curved pipes, *Proceedings of the Royal Society of London, Series A*, Vol. 84, 1910, pp. 107-118

[2] Eustice J., Experiments on stream-line motion in curved pipes, *Proceedings of the Royal Society of London, Series A*, Vol. 85, 1911, pp. 119-131

[3] Dean W. R., Fluid motion in a curved channel, *Proceedings of the Royal Society of London Series A*, Vol. 121, 1928, pp. 402-420

[4] Dean W. R., The stream-line motion of fluid in a curved pipe, *The London, Edinburgh & Dublin Philosophical Magazine and Journal of Science*, Vol. 5, 1928, pp. 673-695

[5] Dean W. R., Note on motion of fluid in curved pipes, *The London, Edinburgh & Dublin Philosophical Magazine and Journal of Science*, Vol. 4, 1927, pp. 208-223

[6] Wang C. C., Chen I. Y. and Huang P. S., Two-phase slug flow across small diameter tubes with the presence of vertical return bend, *International Journal of Heat and Mass Transfer*, Vol. 48, 2005, pp. 2342-2346

[7] Wang C. C., Chen I. Y., Lin Y. T. and Chang Y. J., A visual observation of the air-water two-phase flow in small diameter

tubes subject to the influence of vertical return bends, *Chemical Engineering Research & Design,* Vol. 86, 2008, pp. 1223-1235
[8] Wang C. C., Chen I. Y., Yang Y. W. and Chang Y. J., Two-phase flow pattern in small diameter tubes with the presence of horizontal return bend, *International Journal of Heat and Mass Transfer,* Vol. 46, 2003, pp. 2975-2981
[9] De Kerpel K., Ameel B., Huisseune H., T'Joen C., Canière H. and De Paepe M., Two-phase flow behaviour and pressure drop of R134a in a smooth hairpin, *International Journal of Heat and Mass Transfer,* Vol. 55, 2012, pp. 1179-1188
[10] Silva Lima R. J. D. and Thome J. R., Two-phase flow patterns in U-bends and their contiguous straight tubes for different orientations, tube and bend diameters, *International Journal of Refrigeration-Revue Internationale Du Froid,* Vol. 35, 2012, pp. 1439-1454
[11] Padilla M., Revellin R. and Bonjour J., Two-phase flow visualization and pressure drop measurements of HFO-1234yf and R-134a refrigerants in horizontal return bends, *Experimental Thermal and Fluid Science,* Vol. 39, 2012, pp. 98-111
[12] Canière H., Flow Pattern Mapping of Horizontal Evaporating Refrigerant Flow Based on Capacitive Void Fraction Measurements, PhD thesis, Ghent University, Ghent, Belgium, 2009
[13] Yang S. X. and Yang W. Q., A portable stray-immune capacitance meter, *Review of Scientific Instruments,* Vol. 73, 2002, pp. 1958-1961
[14] Silva Lima R. J. and Thome J. R., Two-Phase Pressure Drops in Adiabatic Horizontal Circular Smooth U-Bends and Contiguous Straight Pipes (RP-1444), *HVAC&R Research,* Vol. 16, 2010, pp. 383-397
[15] Quiben J. M. and Thome J. R., Flow pattern based two-phase frictional pressure drop model for horizontal tubes, Part II: New phenomenological model, *International Journal of Heat and Fluid Flow,* Vol. 28, 2007, pp. 1060-1072
[16] Percival D. B. and Walden A. T., Wavelet methods for time series analysis, Cambridge University Press, New York, Vol. 2000, pp. 594
[17] De Kerpel K., De Keulenaer T., De Schampheleire S. and De Paepe M., Capacitance sensor measurements of upward and downward two-phase flow in vertical return bends, *International Journal of Multiphase Flow-Under Review,* Vol. 2014, pp.
[18] Schubring D. and Shedd T. A., Wave behavior in horizontal annular air-water flow, *International Journal of Multiphase Flow,* Vol. 34, 2008, pp. 636-646